Journal of Alloys and Compounds 763 (2018) 916–925

Contents lists available at ScienceDirect

Journal of Alloys and Compounds

journal homepage: http://www.elsevier.com/locate/jalcom

Intrinsic magnetic properties of $Ce_2(Fe, Co)_{14}B$ and its modifications by Ni and Cu

Tian Wang, Mamoun Medraj*

Department of Mechanical and Industrial Engineering, Concordia University, 1455 de Maisonneuve Boul. West, Montreal, QC H3G 1M8, Canada

ARTICLE INFO

Article history:
Received 29 March 2018
Received in revised form
19 May 2018
Accepted 2 June 2018
Available online 4 June 2018

Keywords:
Permanent magnets
Magnetic measurement
Magnetic $Ce_2Fe_{14-x}Co_xB$
Saturation magnetization
Anisotropy field
Curie temperature

ABSTRACT

The intrinsic magnetic properties of $Ce_2Fe_{14-x}Co_xB$ ($x \leq 4.76$) are studied at 25 °C using key alloys annealed at 900 °C for 25 days. The saturation magnetization (M_s) and the Curie temperature (T_c) of $Ce_2Fe_{14-x}Co_xB$ increase with Co content. However, the anisotropy field (H_a) of $Ce_2Fe_{14-x}Co_xB$ diminishes precipitously with Co content. The process of crystal structure refinement indicates that the saturation magnetization of $Ce_2Fe_{14-x}Co_xB$ is related to the site occupancy of Co atoms at different Fe atomic sites. Co atoms prefer to occupy 8*j2* site, followed by 16*k2*, 4*e* and 16*k1* sites sequentially. Moreover, Co atoms occupying 8*j2* site are more effective leading to an increase in the M_s. The individual effects of Ni or Cu on the intrinsic magnetic properties of $Ce_2Fe_{12.98-x}Co_{1.02}Ni_xB$ and $Ce_2Fe_{12.98-y}Co_{1.02}Cu_yB$ are evaluated. The maximum solid solubilities of Ni and Cu in $Ce_2Fe_{12.98}Co_{1.02}B$ at 900 °C are found to be 8 at.% and 0.8 at.%, respectively. Ni or Cu enhances T_c, but decreases both M_s and H_a of $Ce_2Fe_{12.98}Co_{1.02}B$. The paper also discussed the combined effects of Ni and Cu on the intrinsic magnetic properties of $Ce_2Fe_{12.98}Co_{1.02}B$. The M_s of $Ce_2Fe_{12.98-x-y}Co_{1.02}Ni_xCu_yB$ ($0 \leq x \leq 0.41$, $y \approx 0.119$) increases after doping with both Ni and Cu, reaching around 155 emu/g. Meanwhile, the H_a and the T_c are measured to be near 24 kOe and 280 °C, respectively.

1. Introduction

Rare-earth (RE) based permanent magnets exhibit considerably higher coercivity and energy product than the traditional AlNiCo alloys and hard ferrites [1]. The discovery of $Nd_2Fe_{14}B$-based permanent magnets made it possible for crucial energy efficient technologies such as wind turbines, hybrid vehicle motors and others to come into existence [2]. The growing demand in the world for permanent magnets and the rising costs of the less abundant rare earth metals, including Sm and Dy, necessitates the development of new Fe-based magnets using a relatively abundant and inexpensive rare earth metals such as Ce. Despite the inferior magnetic properties of $Ce_2Fe_{14}B$ compared to $Nd_2Fe_{14}B$, it can still be used in less demanding industrial applications [3]. Co was recognized as a potential additive to improve Curie temperature of $Ce_2Fe_{14}B$ in order to enable its use at high working temperatures [4]. Thus, the Ce-Fe-Co-B system proves to be promising with regard to magnetic phases, especially in the Fe-rich corner, displaying superior magnetic properties to ferrite. For example, the M_s should be higher than 80 emu/g which is the M_s value of $CoFe_2O_4$ [5], and the Curie temperature should be high enough to maintain magnetic performance with increasing temperature as well as having low cost for the automotive or electromechanical applications.

It was reported that magnetic $Ce_2Fe_{14-x}Co_xB$ ($0 \leq x \leq 4.76$) is formed in the Ce-Fe-Co-B system [6]. To introduce a practical hard magnet, the most important step is the determination of its intrinsic magnetic properties. If the results are encouraging, further development can be implemented [7]. However, limited information can be found regarding the intrinsic magnetic properties of $Ce_2(Fe, Co)_{14}B$ in the literature. Moreover, it is essential to understand how the magnetic properties change within the solubility limit of Co in the $Ce_2Fe_{14}B$ compound. Hence, these properties are determined in this study for $Ce_2Fe_{14-x}Co_xB$ ($0 \leq x \leq 4.76$) through the analysis of bulk homogenized alloys.

In the development of magnets, additives are always used for the enhancement of their magnetic properties as well as their thermal stability [8]. However, in many cases, certain properties of permanent magnets are improved by additives while other properties may worsen further. In most permanent magnets, a secondary phase is required to prevent the formation of reverse

* Corresponding author.
E-mail address: mmedraj@encs.concordia.ca (M. Medraj).

https://doi.org/10.1016/j.jallcom.2018.06.017
0925-8388/

magnetic domains that demagnetize the material [8]. The additives modify the nature of the dominating magnetic phases and the composition of the intergranular secondary phases which thereby influencing the microstructure and the properties. The presence of Ni and Cu was reported to be beneficial to the magnetic properties of $Nd_2Fe_{14}B$ magnets, in particular for improving their thermal stability [8–10]. Orimoloye et al. [17] used a similar methodology to the current work to measure the intrinsic magnetic properties of (Al, Ni or Si)-doped $Ce_2Fe_{14}B$. However unlike the current work, they used different additives to modify $Ce_2Fe_{14}B$ without doping it with Co first. They found that Al, Ni, and Si are detrimental to the saturation magnetization and the anisotropy field; whereas, Ni and Si improve the Curie temperature of $Ce_2Fe_{14}B$. So far, limited literature data can be found regarding the effects of these additives on $Ce_2(Fe, Co)_{14}B$. In order to aid the development of Ce-containing permeant magnets, this paper will attempt to understand the effects of Ni and Cu along with Co on the intrinsic magnetic properties of $Ce_2(Fe, Co)_{14}B$.

2. Experimental procedure

Polycrystalline $Ce_2(Fe, Co)_{14}B$, $Ce_2(Fe, Co, Ni)_{14}B$, $Ce_2(Fe, Co, Cu)_{14}B$ and $Ce_2(Fe, Co, Ni, Cu)_{14}B$ alloys were prepared under argon atmosphere using an arc-melting furnace which is equipped with a water-cooled copper crucible and a non-consumable tungsten electrode. Constituent elements with a purity of 99 wt% or higher were used as starting materials. All the elements were supplied by Alfa Aesar® (Haverhill, MA, USA). Every alloy had to be molten several times to ensure homogeneity. The as-cast alloys were then encapsulated inside quartz tubes under vacuum for the process of annealing. After sufficient annealing time, which ranged from 20 to 25 days, the alloys were quenched in a cold-water bath in order to obtain a homogenized structure. The actual global compositions of the alloys were determined by means of the Scanning Electron Microscope (SEM) (HITACHI S-3400N, HITACHI, Tokyo, Japan) coupled with the Energy Dispersive X-ray Spectroscopes (EDS) using area mapping. Three maps were taken for each sample. Further, the difference between the three scans was studied, which was found to be less than ±2 at.% for all the elements. The quenched samples were cut into several pieces. One piece was grinded and polished down to 1 μm to be analyzed by an SEM coupled with a Wavelength Dispersive X-ray Spectroscopes (WDS). A few pieces were crushed into fine powder for X-ray Diffraction (XRD) analysis. XRD was performed on the key alloys using the PANAnalytical Xpert Pro X-ray diffractometer (PANAnalytical, Almelo, The Netherlands) with a CuKα radiation at 45 kV and 40 mA. The XRD patterns were analyzed using the X'Pert Highscore plus software [11] and Rietveld analysis. The crystal structure prototypes used in XRD analysis were taken from Pearson's Database [12].

The saturation magnetization and anisotropy field were measured using the Quantum Design Physical Property Measurement System (PPMS-9T, San Diego, CA, USA) at 298 K. The samples were cut into cubic shapes of approximately 25 mg weight. The saturation magnetization was obtained in external field up to 50 kOe. Since Ce-Fe-Co-B is a complex multi-component system, it is extremely difficult to obtain single phase sample, especially because certain magnetic phases such as $Ce_2(Fe, Co)_{14}B$ form through a peritectic reaction [6]. Practically, in order for the magnetic properties of the alloys to be attributed to the magnetic phase, samples should contain at least seventy mass percent of the magnetic phase of interest with certain amounts of secondary phases which could help impeding domain wall motion [3]. In this research, over 80 wt% of the magnetic phase was obtained in all the samples after the annealing process. However, to describe the saturation magnetization precisely, all the M_s results of the $Ce_2Fe_{14}B$ solid solutions (e.g. $M_s^{Ce2Fe14\text{-}xCoxB}$) reported in this paper have been corrected based on the following equation [19]:

$$M_s^{sample} = \left(w_i^{Ce2Fe14-xCoxB} \times M_s^{Ce2Fe14-xCoxB} + w_i^{imp} \times M_s^{imp}\right)/100 \quad (1)$$

where M_s^{sample} is the saturation magnetization of the sample obtained using PPMS; $w_i^{Ce2Fe14\text{-}xCoxB}$ and w_i^{imp} are the weight percentages of $Ce_2Fe_{14\text{-}x}Co_xB$ and impurity respectively, obtained using XRD through Rietveld analysis; M_s^{imp} is the saturation magnetization of the impurity taken from the literature. The magnetic anisotropy field was determined by the Singular Point Detection (SPD) method, using the second derivative of magnetization (d^2M/dH^2) [13–15].

Curie temperature was measured by TA instruments Q50 (New Castle, DE, USA) thermogravimetric analysis (TGA) with a constant magnetic field applied to the sample. Pure Ni was used as a calibration standard. The error in Curie temperature measurement of Ni was observed to be ±3 °C. The Curie temperature of the magnetic compound and its dependence on compositions are studied and discussed in this paper. All the intrinsic magnetic property measurements were repeated two or four times. The differences between the two measurements were noted to be less than 3.2 emu/g for M_s, 2.7 kOe for H_a, and 4.1 °C for T_c and the average values were reported.

3. Results and discussion

3.1. Intrinsic magnetic properties of $Ce_2Fe_{14\text{-}x}Co_xB$

The ferromagnetic tetragonal $P42/mnm$ $Ce_2Fe_{14}B$ has attracted the attention of researchers hoping to build low cost magnets with acceptable magnetic properties suitable for automobile applications. The Co substitution for Fe enhanced the thermal stability of $Ce_2Fe_{14\text{-}x}Co_xB$ [4]. The maximum solubility of $Ce_2Fe_{14\text{-}x}Co_xB$ was reported as 28 at.% Co ($x = 4.76$) at 900 °C [6]. The details of the influence of Co substitution on the lattice parameters and lattice volume of $Ce_2Fe_{14\text{-}x}Co_xB$ can be found in Refs. [6,19]. Seven key alloys named KAs 1 to 7 were prepared along the homogeneity range of $Ce_2Fe_{14\text{-}x}Co_xB$ by substituting different amounts of Fe with Co. The dominating $Ce_2(Fe, Co)_{14}B$ along with a small amount of impurities (such as α-(Fe, Co)) were obtained after the annealing process. Based on the WDS analysis, α-(Fe, Co) was found to dissolve up to 28 at.% Co. The M_s of α-(Fe, Co) at around 0, 10, 20, 30 at.% Co were reported to vary from 205 to 225 emu/g [18]. The M_s value of $Ce_2Fe_{14\text{-}x}Co_xB$ with different amounts of Co content is calculated using equation (1).

The influence of compositional variations on the intrinsic properties of $Ce_2Fe_{14\text{-}x}Co_xB$ has been studied and presented in Table 1. The magnetic measurements of $Ce_2Fe_{14\text{-}x}Co_xB$ were also compared with the dopant-free $Ce_2Fe_{14}B$ reference material. The compositional dependence of saturation magnetization, anisotropy field and Curie temperature of $Ce_2Fe_{14\text{-}x}Co_xB$ are plotted in Figs. 1 and 2. The dotted lines in these figures are an approximate fit of the data.

The M_s and H_a of dopant-free $Ce_2Fe_{14}B$ are determined in this study, which are also consistent with the results of Orimoloye et al. [17]. The M_s of dopant-free $Ce_2Fe_{14}B$ at 25 °C is measured as 130 emu/g which is approximately 982.8 kA/m using the density of $Ce_2Fe_{14}B$ reported in Ref. [16]. This value is observed to be around 5% greater than the 931.1 kA/m reported by Herbst et al. [3] for $Ce_2Fe_{14}B$ at 22 °C. Such a difference may be due to the contribution of secondary phases such as α-Fe, which is also observed by Kayode et al. [17]. The H_a of dopant-free $Ce_2Fe_{14}B$ is measured as 28.1 kOe

Table 1
Dependence of intrinsic magnetic properties of $Ce_2Fe_{14-x}Co_xB$ on Co content.

Key alloy	Global composition (at.%)	Co content in $Ce_2Fe_{14-x}Co_xB$		M_s (emu/g) at 25 °C	H_a (kOe) at 25 °C	T_c (°C)
		at.%	x			
$Ce_2Fe_{14}B$	$Ce_{13.4}Fe_{80.0}B_{6.6}$	0	0	130.0	28.1	151 [16]
KA 1	$Ce_{13.2}Fe_{76.8}Co_{3.1}B_{6.9}$	3	0.51	133.9	29.2	227
KA 2	$Ce_{14.6}Fe_{72.8}Co_{6.7}B_{5.9}$	6	1.02	140.1	29.3	234
KA 3	$Ce_{15.3}Fe_{67.6}Co_{9.3}B_{7.8}$	9	1.53	145.1	25.5	271
KA 4	$Ce_{13.5}Fe_{69.6}Co_{12.3}B_{4.6}$	14	2.38	149.3	22.7	313
KA 5	$Ce_{14.7}Fe_{59.2}Co_{17.8}B_{8.3}$	18	3.06	153.8	21.7	351
KA 6	$Ce_{13.4}Fe_{61.1}Co_{20.3}B_{5.2}$	22	3.74	154.8	19.4	405
KA 7	$Ce_{13.7}Fe_{53}Co_{30.5}B_{4.9}$	28	4.76	155.1	13.2	467

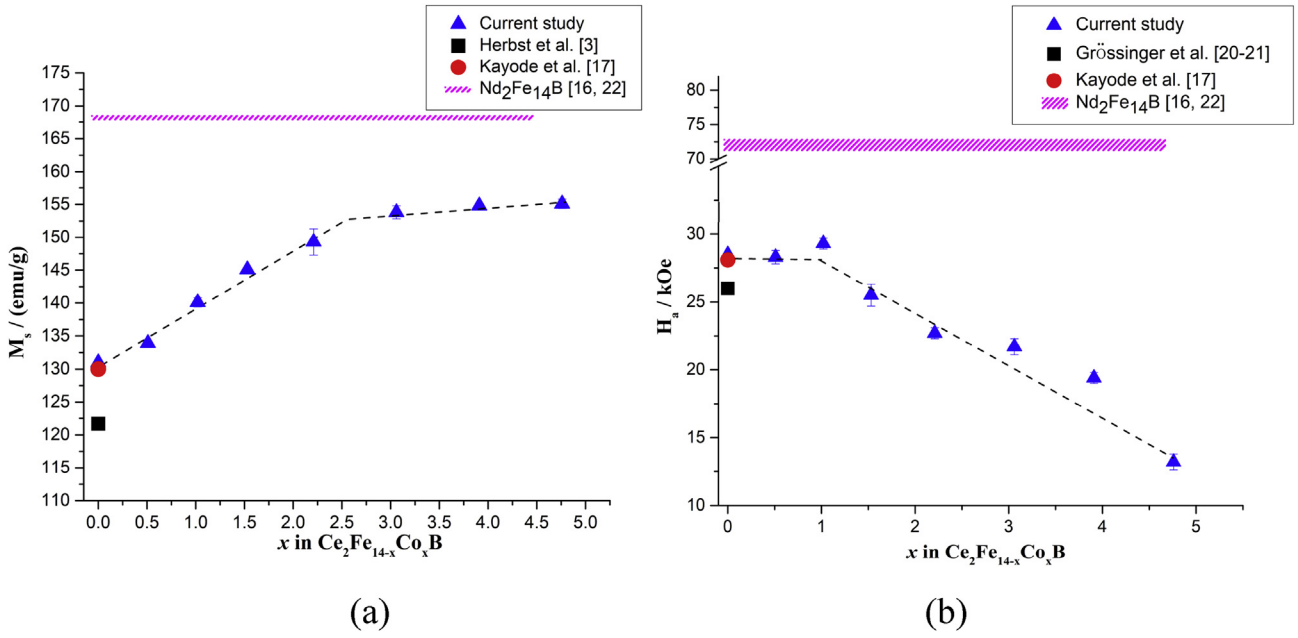

Fig. 1. Compositional dependence of (a) saturation magnetization; (b) anisotropy field of $Ce_2Fe_{14-x}Co_xB$ at 25 °C. The thickness of $Nd_2Fe_{14}B$ line represents the variation in the literature data.

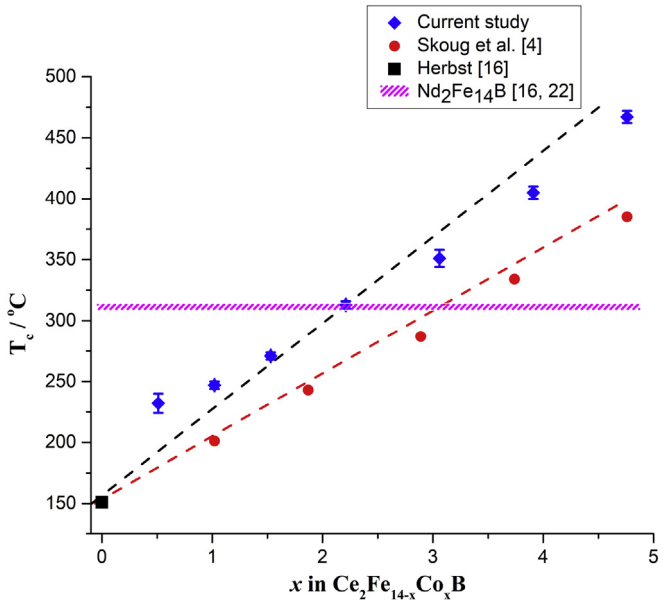

Fig. 2. Current Curie temperature measurements in relation to Skoug et al. [4], Herbst [16] and Huang et al. [22].

which is 8% higher than the 26.0 kOe value reported in the literature [20,21]. As shown in Fig. 1 (a), the saturation magnetization of $Ce_2Fe_{14-x}Co_xB$ is enhanced by Co substitution and becomes closer to that of $Nd_2Fe_{14}B$. By substituting 3 at.% Co ($x = 0.51$) for Fe, the M_s was measured as 133.9 emu/g, which is higher than that of the dopant-free $Ce_2Fe_{14}B$ compound. And the M_s increased by approximately 1.32 emu/g for each 1 at.% substitution of Fe by Co up to 18 at.% Co ($x \leq 3.06$). However, the M_s value of $Ce_2Fe_{14-x}Co_xB$ did not increase considerably when the Co content was over 18 at.% and the rate was around 0.13 emu/g per 1 at.% Co. $Ce_2Fe_{14-x}Co_xB$ was observed to have the highest M_s value of 155.1 emu/g upon reaching the solubility limit of 28 at.% Co ($x = 4.76$). With the influence of Co, the observed M_s value of $Ce_2Fe_{14-x}Co_xB$ exhibited a different tendency compared to that of $R_2(Fe, Co)_{14}B$ (R = Y, Nd and Gd) in Ref. [22]. The M_s dropped proportionally with the Co content in $R_2(Fe, Co)_{14}B$ (R = Y, Nd and Gd). On the other hand, the M_s of $Ce_2Fe_{14-x}Co_xB$ showed an increasing trend with Co. This different behavior might be due to the hybridization between the Ce 4*f* and Co 3d states which results in a strong induced polarization of Ce (4*f*+5d) states that brings large orbital moments at the Ce sites [23]. Also, the influence of Co on the saturation magnetization of $Ce_2Fe_{14-x}Co_xB$ could be related to the Co occupancy on different Fe sites, which will be discussed in the next section.

The anisotropy field of $Ce_2Fe_{14-x}Co_xB$ with 3 at.% Co ($x = 0.51$) was comparable to dopant-free $Ce_2Fe_{14}B$ and it showed a slightly increase to 29.3 kOe in the presence of 6 at.% Co ($x = 1.02$). However, it is still inferior to that of $Nd_2Fe_{14}B$ as shown in Fig. 1 (b). Beyond this composition, H_a of $Ce_2Fe_{14-x}Co_xB$ dropped monotonically with Co concentration. It decreased nearly at about 0.7 kOe for each 1 at.% substitution of Fe by Co. This behavior reflects the reduction of the uniaxial magnetocrystalline anisotropy which was reported by Ref. [4]. The decrease in the magnetic anisotropy of $Ce_2Fe_{14-x}Co_xB$ with Co content is related to the lattice volume shrinkage [6]. Co substitution leads to a reduction in the size of $Ce_2Fe_{14-x}Co_xB$ particles. Large particles reduce the contributions of crystal-symmetry which thereby influences the shape anisotropy and decreases the global anisotropy [6]. The influences of Co content on the anisotropy field and Curie temperature of $Ce_2Fe_{14-x}Co_xB$ are presented in Table 1. In general, Co substitution reduces the anisotropy field but increases the Curie temperature as well as the saturation magnetization of $Ce_2Fe_{14-x}Co_xB$.

The Curie temperature of dopant-free $Ce_2Fe_{14}B$ was reported to be 151 °C [16]. Based on the current observation, the Curie temperature of $Ce_2Fe_{14-x}Co_xB$ increased proportionally with Co concentration, approximately 11.3 °C for each 1 at.% Fe substituted by Co from pure $Ce_2Fe_{14}B$ to $Ce_2Fe_{9.24}Co_{4.76}B$ as shown in Fig. 2. This is principally because the Co-Co exchange interaction is stronger than that of Co-Fe or Fe-Fe interactions [24]. As more Co ions are distributed into the lattice, the Fe-Fe interactions are gradually replaced by Co-Fe and then by Co-Co, which leads to an enhancement of the Curie temperature of $Ce_2Fe_{14-x}Co_xB$. The maximum T_c was measured as 467 °C at 28 at.% Co ($x = 4.76$), surpassing the value of the un-doped $Nd_2Fe_{14}B$ compound, as can be seen in Fig. 2. A similar study has been done by Skoug et al. [4], where the Curie temperature of $Ce_3Fe_{14-x}Co_xB$ melt-spun ribbons was measured. They found that the Curie temperature increased almost uniformly with the Co content in the range of 6–28 at.% ($1.02 \leq x \leq 4.76$). After a comparison of their results [4] with the current work in Fig. 2, a similar trend was observed in both, as the T_c increases almost linearly with the Co content. However, in the current study, Curie temperature of $Ce_2Fe_{14-x}Co_xB$ is, on an average 50 °C higher than that reported in Ref. [4]. The differences in Curie temperature of nanomaterials and bulk polycrystalline materials was also reported by Dominguez et al. [25]. They found as a result of the effect of particle size, the Curie temperature of $CoFe_2O_4$ nanoparticles was observed to be less than that of bulk materials [25]. A similar finding in this study with regard to the difference in Curie temperature suggested that such difference could be due to the particle size effect. The melt-spun ribbons were found to contain smaller grains compared to the annealed polycrystalline bulk materials [25]. In melt-spun materials, fluctuations of electron spins become more prominent, which could potentially reduce the magnetic exchange interaction. Thus, the order-disorder transition of magnetic moments in melt-spun ribbons could be achieved at a relatively lower temperature than the bulk materials, which leads to the lower Curie temperature [25].

The M_s of $Nd_2Fe_{14}B$ was reported as 16 kG (167.6 emu/g) at 22 °C with H_a of 71–73 kOe and T_c of around 312 °C [16,22]. By substitution of Co for Fe in $Ce_2Fe_{14-x}Co_xB$, the M_s and T_c were largely enhanced. The M_s of $Ce_2Fe_{14-x}Co_xB$ is shown to be comparable to $Nd_2Fe_{14}B$, and even the T_c is observed to be greater when containing Co content over 14 at.% ($x \geq 2.38$), as can be seen in Fig. 1 (a) and 2. This indicates that Co-doped $Ce_2Fe_{14}B$ is a promising permanent magnet candidate which should be considered for further development. Hence, Co-containing $Ce_2Fe_{14}B$ solid solutions form the basis for the rest of the analysis presented in this paper. In general, $Ce_2Fe_{14-x}Co_xB$ with 28 at.% Co ($x = 4.76$) manifests the highest saturation magnetization and Curie temperature, but with the lowest anisotropy field. When selecting a potential permanent magnet for certain applications, an intermediate composition between 3 and 18 at.% Co ($0.51 \leq x \leq 3.06$) with high Curie temperature and saturation magnetization but with acceptable anisotropy field might be the most suitable.

3.2. Crystal structure refinement of $Ce_2Fe_{14-x}Co_xB$

The preference of Co occupancies on six crystallographically inequivalent Fe sites of $Nd_2(Fe, Co)_{14}B$ have been studied by Liao et al. [26]. Their results clearly indicate that Co prefers the 8*j2* and 16*k2* sites. Besides, Co atoms were seen to strongly avoid the 8*j1* site. The 16*k1* and 4*e* sites were observed to be randomly populated by the remaining Co atoms, while they also showed a small avoidance concerning the 4*c* site [26]. All the sites avoided by Co were found to be associated with the largest iron hyperfine fields, while the preferred sites tended to be those with small hyperfine fields [26]. It is known that the change of the average atomic size, caused by replacing Fe atoms with others, can be correlated with the change in the effective magnetic moment of hyperfine fields [27]. Therefore, it can be said that as the magnetic moment of the magnetic phase is associated with Fe atoms, whereas the change in the value of hyperfine fields caused by additives is related to the change in the magnetic moment [26]. This explains why modest Co additions to iron-based magnetic alloys generally lead to an increase in magnetization.

Table 2 presents the refined crystal structure parameters of $Ce_2Fe_{14-x}Co_xB$ and its reliability factors. The current refinement of structure parameters of $Ce_2Fe_{14-x}Co_xB$ shows consistent results with the study of $Nd_2Fe_{14-x}Co_xB$ in Ref. [26]. The decrease in the unit cell parameters is in favor of the Co occupancy at 8*j2* site. The prerequisite substitutional position of 8*j2* site has also been confirmed by the shortest lengths of Fe-Fe bond as can be seen in Table 3. Most of the bond lengths with Fe4 show relatively short distance, indicating that the Fe4 position has higher potential to be substituted by the Co smaller atoms because shorter distance results in higher potential energy and more reactivity. Therefore, replacing Fe4 by Co atoms lowers the total energy enabling the materials to reach equilibrium. Once the 8*j2* site are completely occupied by Co atoms, Fe atoms start to be replaced sequentially by Co on 16*k2*, 4*e*, and 16*k1* sites.

The fractional atomic occupancy of 8*j2*, 16*k2*, 4*e* and 16*k1* sites of $Ce_2Fe_{14-x}Co_xB$ have been determined as a function of Co concentration which has been presented in Fig. 3. When adding Co and Ni, the reduction in effective magnetic hyperfine fields is proportional to the electrons number in partially filled 3d and 4d shell [28]. On the other hand, when adding Cu, the reduction in the effective magnetic hyperfine fields is directly proportional to the number of electrons in the outer electron shell and inversely proportional to the number of electrons of the additive element [28]. As Co occupies the Fe sites with low hyperfine fields, an increase of saturation magnetization of magnetic phase is achieved. Relating Fig. 3 to the saturation magnetization of $Ce_2Fe_{14-x}Co_xB$ in Fig. 1 (a), an increase is observed in saturation magnetization when $x \leq 2.38$ is related to the continuous occupancy of Co atoms at 8*j2* site. Later, the Co occupancy at other Fe sites does not influence the saturation magnetization significantly. However, the Co substitution in the unit cell leads to a stronger average exchange interaction which may be responsible for the significantly higher Curie temperature [29] and for the continuous increase of its value with Co concentration. The coordination spheres and atomic substitution of Fe by

Table 2
Refined crystal structure parameters of $Ce_2Fe_{14-x}Co_xB$.

Sample No.	Wyckoff position	Atomic position			Occupancy (%)	Reliability factors[a]		
		x	*y*	*z*		R_e	R_{wp}	*s*
KA 1	Fe1-16*k1*	0.0671	0.2765	0.1269	Fe 100.0	19.48	23.07	0.71
	Fe2-16*k2*	0.0379	0.3587	0.3237	Fe 100.0			
	Fe3-8*j1*	0.3174	0.3174	0.2535	Fe 100.0			
	FeCo4-8*j2*	0.0979	0.0979	0.2951	Co 27.1			
	Fe5-4*e*	0	0	0.1144	Fe 100.0			
	Fe6-4*c*	0	0.5	0	Fe 100.0			
	Ce1-4g	0.2313	0.7687	0	Ce 100.0			
	Ce2-4*f*	0.3585	0.3585	0	Ce 100.0			
	B-4*f*	0.1243	0.1243	0	B 100.0			
KA 2	Fe1-16*k1*	0.0671	0.2765	0.1269	Fe 100.0	21.06	23.66	0.79
	Fe2-16*k2*	0.0379	0.3587	0.3237	Fe 100.0			
	Fe3-8*j1*	0.3174	0.3174	0.2535	Fe 100.0			
	FeCo4-8*j2*	0.0979	0.0979	0.2951	Co 53.2			
	Fe5-4*e*	0	0	0.1144	Fe 100.0			
	Fe6-4*c*	0	0.5	0	Fe 100.0			
	Ce1-4g	0.2313	0.7687	0	Ce 100.0			
	Ce2-4*f*	0.3585	0.3585	0	Ce 100.0			
	B-4*f*	0.1243	0.1243	0	B 100.0			
KA 3	Fe1-16*k1*	0.0671	0.2765	0.1269	Fe 100.0	22.25	30.03	1.82
	Fe2-16*k2*	0.0379	0.3587	0.3237	Fe 100.0			
	Fe3-8*j1*	0.3174	0.3174	0.2535	Fe 100.0			
	FeCo4-8*j2*	0.0979	0.0979	0.2951	Co 82.9			
	Fe5-4*e*	0	0	0.1144	Fe 100.0			
	Fe6-4*c*	0	0.5	0	Fe 100.0			
	Ce1-4g	0.2313	0.7687	0	Ce 100.0			
	Ce2-4*f*	0.3585	0.3585	0	Ce 100.0			
	B-4*f*	0.1243	0.1243	0	B 100.0			
KA 4	Fe1-16*k1*	0.0671	0.2765	0.1269	Fe 100.0	21.86	29.31	1.79
	FeCo2-16*k2*	0.0379	0.3587	0.3237	Co 0.6			
	Fe3-8*j1*	0.3174	0.3174	0.2535	Fe 100.0			
	Co4-8*j2*	0.0979	0.0979	0.2951	Co 100.0			
	Fe5-4*e*	0	0	0.1144	Fe 100.0			
	Fe6-4*c*	0	0.5	0	Fe 100.0			
	Ce1-4g	0.2313	0.7687	0	Ce 100.0			
	Ce2-4*f*	0.3585	0.3585	0	Ce 100.0			
	B-4*f*	0.1243	0.1243	0	B 100.0			
KA 5	Fe1-16*k1*	0.0671	0.2765	0.1269	Fe 100.0	23.96	27.11	1.27
	FeCo2-16*k2*	0.0379	0.3587	0.3237	Co 20.6			
	Fe3-8*j1*	0.3174	0.3174	0.2535	Fe 100.0			
	Co4-8*j2*	0.0979	0.0979	0.2951	Co 100.0			
	Fe5-4*e*	0	0	0.1144	Fe 100.0			
	Fe6-4*c*	0	0.5	0	Fe 100.0			
	Ce1-4g	0.2313	0.7687	0	Ce 100.0			
	Ce2-4*f*	0.3585	0.3585	0	Ce 100.0			
	B-4*f*	0.1243	0.1243	0	B 100.0			
KA 6	Fe1-16*k1*	0.0671	0.2765	0.1269	Fe 100.0	22.98	26.49	1.32
	FeCo2-16*k2*	0.0379	0.3587	0.3237	Co 34.5			
	Fe3-8*j1*	0.3174	0.3174	0.2535	Fe 100.0			
	Co4-8*j2*	0.0979	0.0979	0.2951	Co 100.0			
	FeCo5-4*e*	0	0	0.1144	Co 6.5			
	Fe6-4*c*	0	0.5	0	Fe 100.0			
	Ce1-4g	0.2313	0.7687	0	Ce 100.0			
	Ce2-4*f*	0.3585	0.3585	0	Ce 100.0			
	B-4*f*	0.1243	0.1243	0	B 100.0			
KA 7	FeCo1-16*k1*	0.0671	0.2765	0.1269	Co 3.5	22.64	30.86	1.85
	FeCo2-16*k2*	0.0379	0.3587	0.3237	Co 43.4			
	Fe3-8*j1*	0.3174	0.3174	0.2535	Fe 100.0			
	Co4-8*j2*	0.0979	0.0979	0.2951	Co 100.0			
	FeCo5-4*e*	0	0	0.1144	Co 19.5			
	Fe6-4*c*	0	0.5	0	Fe 100.0			
	Ce1-4g	0.2313	0.7687	0	Ce 100.0			
	Ce2-4*f*	0.3585	0.3585	0	Ce 100.0			
	B-4*f*	0.1243	0.1243	0	B 100.0			

[a] Reliability factors: R_e is the value statistically expected; R_{wp} is the weighted summation of residuals of the least squared fit; *s* presents the goodness of fit.

Co for the different atomic coordinates have been identified and presented in Fig. 4. The sequence of Co substitution on Fe sites gradually occupying 8*j2* site of $Ce_2Fe_{14-x}Co_xB$ is followed by the sequentially occupation of 16*k2*, 4*e* and 16*k1* sites, both of which have been illustrated in this figure.

3.3. Intrinsic magnetic properties of $Ce_2Fe_{12.98-x}Co_{1.02}Ni_xB$ and $Ce_2Fe_{12.98-x}Co_{1.02}Cu_xB$

$Ce_2Fe_{14-x}Co_xB$ with 6 at.% Co ($x = 1.02$) was found to have the highest anisotropy field ($H_a = 29.3$ kOe) with a saturation

Table 3
Atomic Fe-Fe bond lengths of $Ce_2Fe_{14-x}Co_xB$. The bold values represent the shortest atomic Fe-Fe bond.

Atom 1	Atom 2	Distance (Å)
Fe1	Fe5	2.497
Fe1	Fe6	2.554
Fe1	Fe4	2.576
Fe1	Fe1	2.594
Fe1	Fe3	2.696
Fe2	Fe4	**2.369**
Fe2	Fe1	2.454
Fe2	Fe6	2.483
Fe2	Fe2	2.539
Fe2	Fe3	2.616
Fe4	Fe4	**2.426**
Fe4	Fe5	2.494
Fe4	Fe3	2.633
Fe3	Fe5	2.767
Fe5	Fe5	2.760

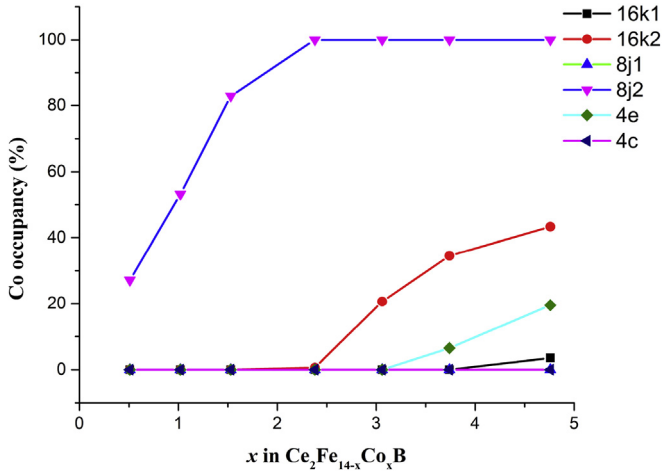

Fig. 3. Co occupancy in $Ce_2Fe_{14-x}Co_xB$ as a function of Co concentration.

magnetization of 140.1 emu/g and Curie temperature of 234 °C in the range between 0 and 28 at.% Co ($0 \leq x \leq 4.76$). According to the research of Fan et al. [30], the substitution of Ni for Co was detrimental to the Curie temperature of the FeCoZrBCu magnet. In order to maintain the thermal stability as well as the high anisotropy field of $Ce_2(Fe, Co)_{14}B$, six Ni-doped $Ce_2(Fe, Co)_{14}B$ alloys were designed by keeping the Co concentration constant at 6 at.%, while substitutions occurred between Fe and Ni. The chemical compositions were presented by the formula of $Ce_2Fe_{12.98-x}Co_{1.02}Ni_xB$. Fe was substituted by around 0.5, 1, 3, 5, 7, 10 and 13 at.% Ni to study the effect of Ni on the intrinsic magnetic properties and measure the homogeneity range of $Ce_2Fe_{12.98-x}Co_{1.02}Ni_xB$ at 900 °C. The dominant $Ce_2Fe_{12.98-x}Co_{1.02}Ni_xB$ was obtained in KAs 8 to 12. As the Ni content increased to 10 at.% in the global composition, the quantity of $Ce_2(Fe, Co, Ni)_{14}B$ reduced significantly due to the formation of other phases. The solid solubility of Ni in $Ce_2Fe_{12.98-x}Co_{1.02}Ni_xB$ was measured to be around 8 at.% ($x = 1.36$) at 900 °C. Traces of $Ce_2(Fe, Co, Ni)_{14}B$ were no longer observed in the alloy containing 12 at.% Ni, and $Ce(Co, Fe, Ni)_4B$ became the dominating phase.

The influence of Ni on the lattice parameters of $Ce_2Fe_{12.98-x}Co_{1.02}Ni_xB$ is illustrated in Fig. 5. The substitution of Fe by Ni, which has a smaller atomic radius, leads to a decrease in the unit cell parameters and the lattice volume. This is confirmed by the increase in 2θ values of the peak positions due to an increase in Ni concentration. The linear relations between the lattice parameters, lattice volume, and Ni concentration obey Vegard's law [31], thereby indicating the occurrence of substitutional solid solubility in $Ce_2Fe_{12.98-x}Co_{1.02}Ni_xB$.

The intrinsic magnetic properties of $Ce_2Fe_{12.98-x}Co_{1.02}Ni_xB$ are summarized in Table 4. Curie temperature of Ni-doped $Ce_2Fe_{12.98-}Co_{1.02}B$ is improved; whereas, the saturation magnetization and the anisotropy field have diminished with the Ni substitution. The compositional dependence of saturation magnetization, anisotropy field, and Curie temperature of $Ce_2Fe_{12.98-x}Co_{1.02}Ni_xB$ are plotted as red triangles in Fig. 6, where the red dotted lines are an approximate fit of the data.

A drop of the M_s value is observed at a rate of 3.82 emu/g per 1 at.% Ni as shown in Fig. 6 (a), which indicates that Ni additive is

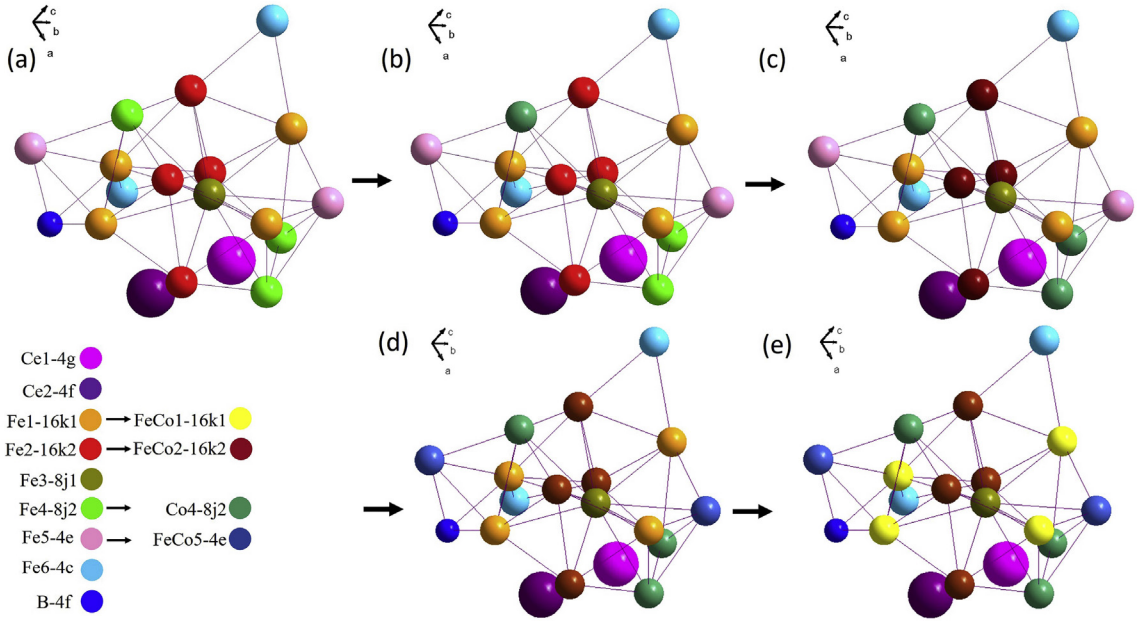

Fig. 4. The coordination spheres of dynamic atomic substitution of Fe by Co with different atomic coordinates: (a) before Co substitution in $Ce_2Fe_{14}B$; (b) to (c) substitution of Fe atoms by Co atoms on 8*j2* site until they are completely occupied by Co and then started to occupy 16*k2* site; (d) to (e) the substitution of Fe by Co atoms on 4*e* and 16*k1* sites.

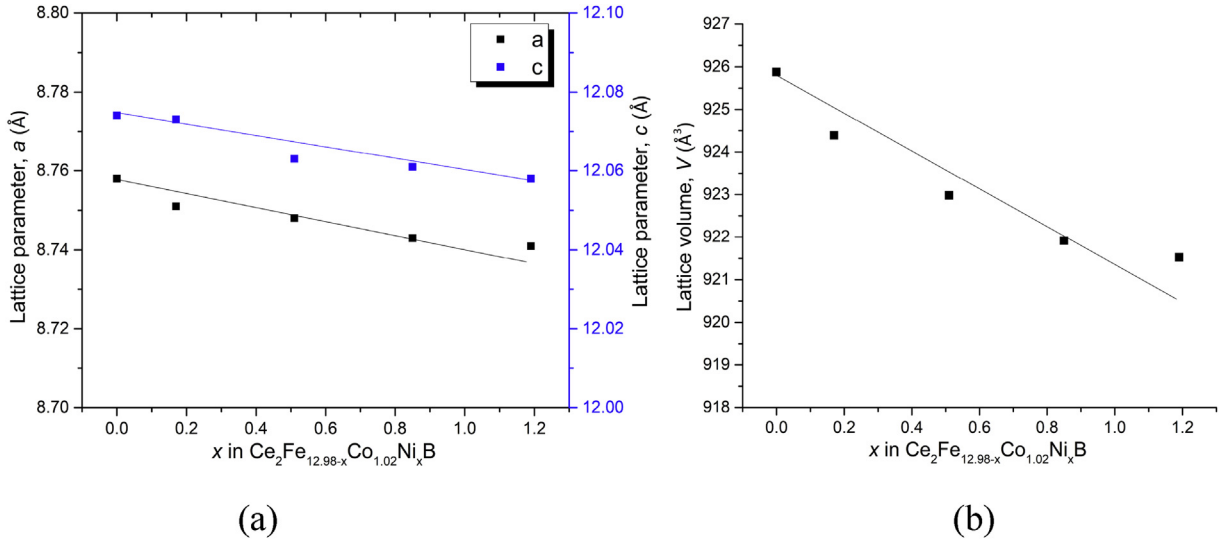

Fig. 5. Cell parameters (a) *a* and *c*; and (b) lattice volume *V* versus Ni concentration in $Ce_2Fe_{12.98-x}Co_{1.02}Ni_xB$.

Table 4
Intrinsic magnetic properties of $Ce_2Fe_{12.98-x}Co_{1.02}Ni_xB$.

Key alloy	Global composition (at.%)	Ni content in $Ce_2Fe_{12.98-x}Co_{1.02}Ni_xB$		M_s (emu/g) at 25 °C	H_a (kOe) at 25 °C	T_c (°C)
		at.%	*x*			
$Ce_2Fe_{12.98-x}Co_{1.02}Ni_xB$	$Ce_{14.6}Fe_{72.8}Co_{6.7}B_{5.9}$	0	0	140.1	29.3	234
KA 8	$Ce_{14.5}Fe_{73.1}Co_{6.1}Ni_{0.5}B_{5.8}$	0.7	0.12	135.2	26.6	261
KA 9	$Ce_{14.8}Fe_{73.9}Co_{5.9}Ni_{1.2}B_{4.2}$	1	0.17	128.0	25.7	265
KA 10	$Ce_{15.1}Fe_{67.1}Co_{6.8}Ni_{3.1}B_{7.9}$	3	0.51	124.8	24.5	278
KA 11	$Ce_{13.5}Fe_{67.4}Co_{6.4}Ni_{5.4}B_{7.3}$	5	0.85	115.7	23.8	293
KA 12	$Ce_{12.7}Fe_{66.9}Co_{6.5}Ni_{7.3}B_{6.6}$	7	1.19	113.3	22.6	297

detrimental to the saturation magnetization of $Ce_2Fe_{12.98}Co_{1.02}B$. A similar phenomenon was also observed by Bolzoni et al. [9]. They analyzed three Ni-doped $Nd_2Fe_{14}B$ alloys, where the M_s value was reported to drop from 187 to 180 emu/g at 77 K after dissolving around 6 at.% Ni. Ni reducing the saturation magnetization of $Nd_2(Fe_{1-y}Ni_y)_{14}B$ was explained by the electron transfer between Ni and Nd [12]. Ni prefers to substitute Fe at the 16*k2* and 8*j2* sites simultaneously in $Nd_2(Fe_{1-y}Ni_y)_{14}B$ [32]. The large electronegativity difference between Ni and rare earth atoms [33], and the 16*k2* site occupancy by Ni atoms both result in considerable electron transfer, which thereby leads to the hybridized state commonly observed in RE-Ni compounds [34]. In $Nd_2(Fe_{1-x-y}Co_xNi_y)_{14}B$. The 8*j2* site is separated from the Nd-B layers by the iron atomic layer as can be seen in Fig. 4. Hence, the electron transfer does not take place after the Ni occupancy and the saturation magnetization of $Nd_2(Fe_{1-x-y}Co_xNi_y)_{14}B$ is only affected by the Co content and the occupancy of Co atoms at this site [35]. In our case, the double substitution of Co and Ni for Fe atoms could further impact the electron transfer in the crystal. In $Ce_2Fe_{12.98-x}Co_{1.02}Ni_xB$, 8*j2* site has been largely occupied by Co atoms, which leads to the gradual occupancy of Ni atoms at 16*k2* site during the substitution. Since the occupancy of Ni at 8*j2* site does not affect the saturation magnetization, as significantly more Ni atoms occupy 16*k2* site, certain amount of electron transfer occurs, and the saturation magnetization of $Ce_2Fe_{12.98-x}Co_{1.02}Ni_xB$ decreases monotonously with Ni as shown in Fig. 6 (a).

Ni has a low anisotropy constant *K1* of -5.7×10^3 J/m^3, which is far lower than that of Fe (48×10^3 J/m^3) and Co (461×10^3 J/m^3) at room temperature [36]. Thus, Ni substitution for Fe could reduce the effective magneto-crystalline anisotropy of Ni-doped $Ce_2Fe_{12.98}Co_{1.02}B$. The compositional dependence of the anisotropy field at 25 °C is shown in Fig. 6 (b). The H_a value of $Ce_2Fe_{12.98}Co_{1.02}B$ before Ni substitution was measured to be at 29.3 kOe. With the influence of Ni, a drop was observed in the anisotropy field of Ni-doped $Ce_2Fe_{12.98}Co_{1.02}B$. The decrement rate of H_a is determined as 0.96 kOe per 1 at.% Ni. Similarly, Bolzoni et al. [9] found that H_a of $Nd_2Fe_{14-x}Ni_xB$ ($1 \leq x \leq 3$) decreased with the influence of Ni at 293 K.

Ni substitution enhances the Curie temperature of $Nd_2Fe_{14-x}Ni_xB$ [9]. For the current $Ce_2Fe_{12.98-x}Co_{1.02}Ni_xB$, substitution of Ni for Fe increases the Curie temperature significantly, which indicates that the magnetic interactions are highly improved by Ni. The T_c of $Ce_2Fe_{12.98-x}Co_{1.02}Ni_xB$ is improved from 234 °C to around 297 °C after doping with 7 at.% Ni ($x = 1.19$) as can be seen in Fig. 6 (c). The increment rate of T_c is approximately 9 °C per 1 at.% Ni. An overall enhancement of Curie temperature could be observed for $Ce_2Fe_{12.98-x}Co_{1.02}Ni_xB$ in Fig. 6 (c). In general, $Ce_2Fe_{12.98-x}Co_{1.02}Ni_xB$ ($x = 0.12$) has the optimum intrinsic magnetic properties, because it has the highest M_s value (135.2 emu/g) among the Ni-containing alloys with moderate H_a (26.6 kOe) and T_c (261 °C) among all Ni-doped $Ce_2Fe_{12.98}Co_{1.02}B$.

Cu normally locates at the intergranular regions. Through pinning the domain wall movement, Cu is an essential additive that influences the extrinsic magnetic properties of Nd-Fe-B [37]. Therefore, Cu effects on the intrinsic magnetic properties of $Ce_2(Fe, Co)_{14}B$ have to be understood first, especially because this information is scarce in the literature. The Fe-Cu and Co-Cu binary systems are characterized by the presence of a liquid-liquid

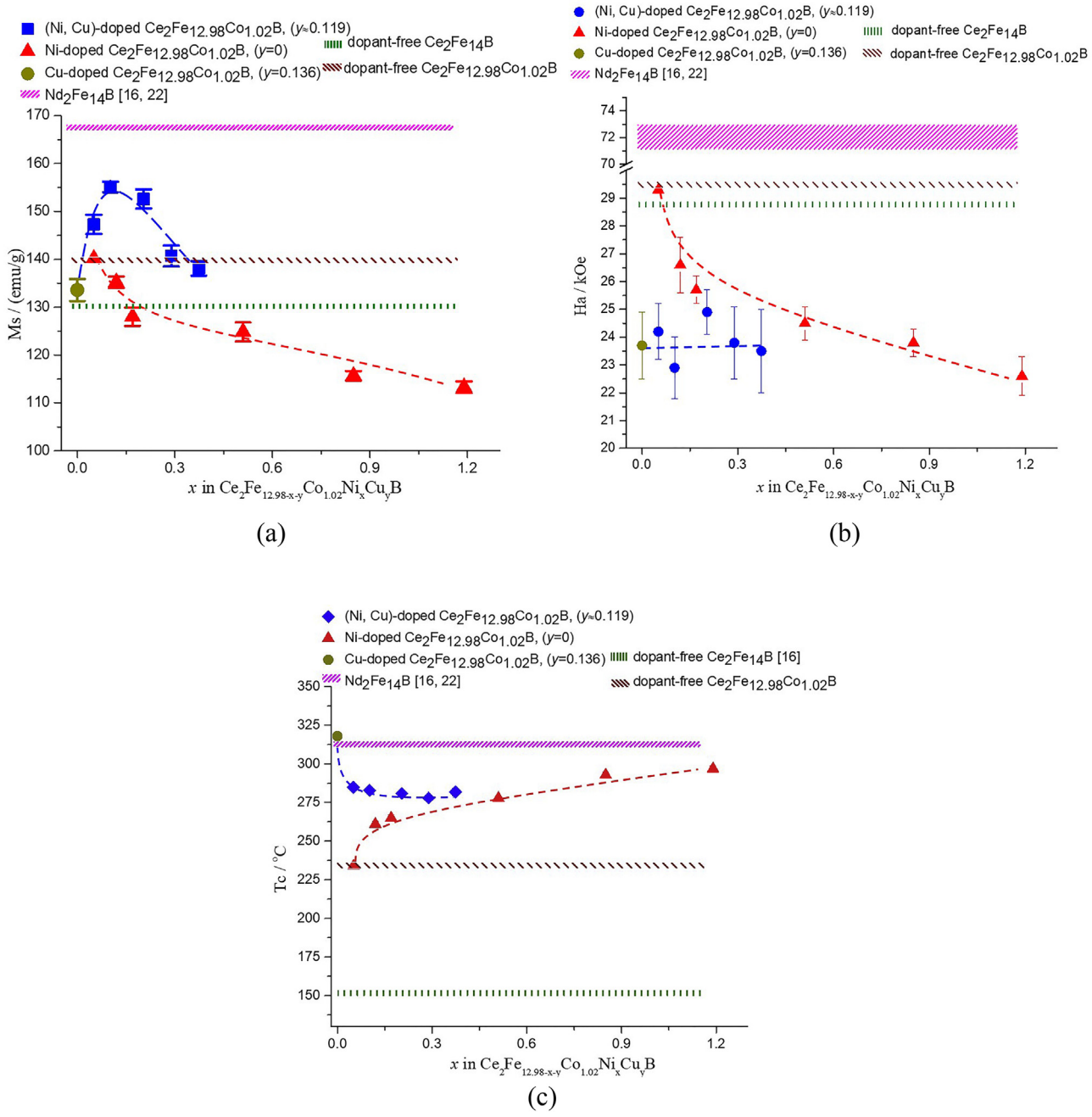

Fig. 6. Compositional dependence of (a) saturation magnetization; (b) anisotropy field; (c) Curie temperature of $Ce_2Fe_{12.98-x-y}Co_{1.02}Ni_xCu_yB$. The thickness of $Nd_2Fe_{14}B$ line represents the variation in the literature data.

miscibility gap [38,39], which leads to the fact that very limited Cu could dissolve in the Fe-rich or Co-rich Ce-Fe-Co-B compounds. Key alloys were designed by varying Cu content in the global compositions of $Ce_2Fe_{12.98-x}Co_{1.02}Cu_xB$ alloys. The maximum solid solubility of $Ce_2Fe_{12.98-x}Co_{1.02}Cu_xB$ was determined as 0.8 at.% Cu ($x = 0.136$) at 900 °C. The intrinsic magnetic properties of $Ce_2Fe_{12.98-x}Co_{1.02}Cu_xB$ ($x = 0.136$) are discussed below.

When $Ce_2Fe_{12.98-x}Co_{1.02}Cu_xB$ contained 0.8 at.% Cu ($x = 0.136$), the Curie temperature increased up to 318 °C. Meanwhile, the saturation magnetization and the anisotropy field decreased from 140.1 emu/g to 133.6 emu/g, and from 29.3 kOe to 23.7 kOe, respectively. As compared to $Ce_2Fe_{12.81}Co_{1.02}Ni_{0.17}B$ which contains similar Ni content as that of Cu, it is obvious that Cu is much more effective in improving Curie temperature than Ni. By doping with Cu, the T_c of $Ce_2Fe_{12.844}Co_{1.02}Cu_{0.136}B$ is observed to be higher than that of Ni-doped $Ce_2Fe_{12.81}Co_{1.02}Ni_{0.17}B$, while the M_s and H_a values of these two compounds were close to each other as can be seen in Table 5 and Fig. 6.

3.4. The combined effects of Ni and Cu on intrinsic magnetic properties of $Ce_2Fe_{12.98-x-y}Co_{1.02}Ni_xCu_yB$

The effects of substituting Fe by both Ni and Cu on the intrinsic magnetic properties of $Ce_2Fe_{12.98}Co_{1.02}B$ were also studied. Six $Ce_2Fe_{12.98-x-y}Co_{1.02}Ni_xCu_yB$ alloys were prepared by keeping the Co content constant at 6 at.%. The contents of Ni and Cu, however,

Table 5
Intrinsic magnetic properties of $Ce_2Fe_{12.98-x}Co_{1.02}Cu_xB$.

Key alloy	Global composition (at.%)	Cu content in $Ce_2Fe_{12.98-x}Co_{1.02}Cu_xB$		M_s (emu/g) at 25 °C	H_a (kOe) at 25 °C	T_c (°C)
		at.%	x			
$Ce_2Fe_{12.98-x}Co_{1.02}Cu_xB$	$Ce_{14.6}Fe_{72.8}Co_{6.7}B_{5.9}$	0	0	140.1	29.3	234
$Ce_2Fe_{12.81}Co_{1.02}Ni_{0.17}B$	$Ce_{14.8}Fe_{73.9}Co_{5.9}Ni_{1.2}B_{4.2}$	0	0	128.0	25.7	271
KA 13	$Ce_{13.2}Fe_{71.6}Co_{6.3}Cu_{1.1}B_{7.8}$	0.8	0.136	133.6	23.7	318

varied in the global compositions as listed in Table 6. Dominating $Ce_2Fe_{12.98-x-y}Co_{1.02}Ni_xCu_yB$ is obtained in all alloys after the process of annealing at 900 °C for 25 days. The Cu overall content was varied in six alloys from 0.7 to 2.8 at.%. Cu solubility in this compound was measured using WDS point analysis on several locations and the average value was reported. In all of the six samples, the maximum Cu solubility was 0.8 at.% in $Ce_2Fe_{12.98-x-y}Co_{1.02}Ni_xCu_yB$. This is also consistent with the results of the Cu-doped $Ce_2Fe_{12.98-x}Co_{1.02}B$ which are discussed in the previous section.

The intrinsic magnetic properties of $Ce_2Fe_{12.98-x-y}Co_{1.02}Ni_xCu_yB$ are summarized in Table 6. It is noticeable that the saturation magnetization and the Curie temperature are improved, while the anisotropy field drops after the double substitution. The optimum intrinsic magnetic properties of $Ce_2Fe_{12.98-x-y}Co_{1.02}Ni_xCu_yB$ were observed to be as follows: $M_s = 152.6$ emu/g, $H_a = 24.9$ kOe and $T_c = 281$ °C, at Ni = 1.2 at.% ($x = 0.204$) and Cu = 0.7 at.% ($y = 0.119$). The intrinsic magnetic properties of (Ni, Cu)-doped $Ce_2Fe_{12.98-x}Co_{1.02}B$ were also compared with the Ni-doped and the Cu-doped $Ce_2Fe_{12.98}Co_{1.02}B$ compound as well as with $Nd_2Fe_{14}B$, which have been depicted in Fig. 6. The Cu content in $Ce_2Fe_{12.98-x-y}Co_{1.02}Ni_xCu_yB$ varied in a limited range between 0.6 and 0.8 at.%. For the purpose of comparison, the Cu contents dissolved in all the $Ce_2Fe_{12.98-x-y}Co_{1.02}Ni_xCu_yB$ solid solutions are considered to be 0.7 at.% ($y \approx 0.119$) in Fig. 6. The intrinsic magnetic properties of $Nd_2Fe_{14}B$, dopant-free $Ce_2Fe_{14}B$ and dopant-free $Ce_2Fe_{12.98}Co_{1.02}B$ are also inserted using pink, green and brown lines in Fig. 6. They represent benchmarks to measure the improvement in the magnetic property improvement after doping with Ni and/or Cu.

Fig. 6 (a) shows the saturation magnetization of $Ce_2Fe_{12.98-x-y}Co_{1.02}Ni_xCu_yB$ in the range of $0 \le x \le 0.41$, $y \approx 0.119$. In general, the M_s of (Ni, Cu)-doped $Ce_2Fe_{12.98}Co_{1.02}B$ is seen to be higher than that of Ni-doped or Cu-doped $Ce_2Fe_{12.98}Co_{1.02}B$ but still inferior to $Nd_2Fe_{14}B$. It first increases with Ni substitution, when Ni content is below 0.6 at.% ($x \le 0.102$). Then, M_s drops at a rate of 9.4 emu/g per 1 at.% Ni after doping with Ni between 0.6 at.% and 2.4 at.% ($0.102 \le x \le 0.408$). Since the Cu content in $Ce_2Fe_{12.98-x-y}Co_{1.02}Ni_xCu_yB$ does not vary considerably, such a decline in the value of M_s may be due to the different site occupancies of Ni at Fe sites. So far, the combination of Ni and Cu demonstrates a significant improvement in the saturation magnetization.

The anisotropy field of $Ce_2Fe_{12.98}Co_{1.02}B$ drops after the individual substitution of Ni or Cu for Fe atoms as shown in Table 6 and Fig. 6 (b). Through the combined substitution of both Ni and Cu in $Ce_2Fe_{12.98-x-y}Co_{1.02}Ni_xCu_yB$ in the range of $0 \le x \le 0.41$, $y \approx 0.119$, the H_a did not change significantly and appeared to be constant at around 23.5 kOe. It is worth noting that both individual and combined substitution have a similar influence on the anisotropy field and the results are comparable to each other, but in fact, they are lower than that of dopant-free $Ce_2Fe_{12.98}Co_{1.02}B$, dopant-free $Ce_2Fe_{14}B$ and much lower than $Nd_2Fe_{14}B$ as can be seen in Fig. 6 (b).

By dissolving around 0.8 at.% Cu ($x = 0.136$) in $Ce_2Fe_{12.98-x}Co_{1.02}Cu_xB$, the highest Curie temperature of 318 °C is achieved. It shows a significant increase as compared to the 234 °C of dopant-free $Ce_2Fe_{12.98}Co_{1.02}B$ and 151 °C [16] of dopant-free $Ce_2Fe_{14}B$. After the combined substitution of Ni and Cu, the T_c of $Ce_2Fe_{12.98-x-y}Co_{1.02}Ni_xCu_yB$ is measured to be around 282 ± 3 °C which is similar to the T_c of Ni-doped $Ce_2Fe_{12.98}Co_{1.02}B$ at $0.51 \le x \le 1.19$ and $Nd_2Fe_{14}B$, but lower than that of Cu-doped $Ce_2Fe_{12.98}Co_{1.02}B$ as can be seen in Fig. 6 (c). Nevertheless, the T_c of (Ni, Cu)-doped $Ce_2Fe_{12.98}Co_{1.02}B$ increased almost 50 °C compared to that of dopant-free $Ce_2Fe_{12.98}Co_{1.02}B$.

4. Conclusions

In this research, the intrinsic magnetic properties of $Ce_2Fe_{14-x}Co_xB$ ($x \le 4.76$) were studied at 25 °C. From the current investigation, the substitution of Co for Fe in the $Ce_2Fe_{14}B$ enhances the M_s and T_c values. Whereas the H_a decreases proportionally with Co concentration. The crystal structure refinement of $Ce_2Fe_{14-x}Co_xB$ reveals that Co atoms show a preferred occupancy at 8*j2* site. After this site is fully occupied, Co atoms start occupying 16*k2*, 4*e* and 16*k1* sites, consecutively. The occupancy of Co at different sites is found to be related to the saturation magnetization of $Ce_2Fe_{14-x}Co_xB$ where the rate of increase in M_s drops after the 8*j2* site is fully occupied. The highest values of M_s and T_c of $Ce_2Fe_{14-x}Co_xB$ are measured to be 155.1 emu/g and 467 °C, at 28 at.% Co ($x = 4.76$). However, the highest H_a is determined as 29.3 kOe, at 6 at.% Co ($x = 1.02$). The substitution of Ni or Cu alone for Fe is unfavorable to the M_s and H_a values of $Ce_2Fe_{12.98}Co_{1.02}B$. However, the T_c of $Ce_2Fe_{12.98}Co_{1.02}B$ can be further improved through substituting by

Table 6
Intrinsic magnetic properties of $Ce_2Fe_{12.98-x-y}Co_{1.02}Ni_xCu_yB$.

Key alloy	Global composition (at.%)	Ni content in $Ce_2Fe_{12.98-x-y}Co_{1.02}Ni_xCu_yB$		Cu content in $Ce_2Fe_{12.98-x-y}Co_{1.02}Ni_xCu_yB$		M_s (emu/g) at 25 °C	H_a (kOe) at 25 °C	T_c (°C)
		at.%	x	at.%	y			
$Ce_2Fe_{12.98}Co_{1.02}B$	$Ce_{14.6}Fe_{72.8}Co_{6.7}B_{5.9}$	0	0	0	0	140.1	29.3	234
KA 14	$Ce_{13.1}Fe_{71.6}Co_{6.1}Ni_{0.3}Cu_{2.8}B_{6.1}$	0.3	0.051	0.8	0.136	147.3	24.2	285
KA 15	$Ce_{10.3}Fe_{74.9}Co_{6.0}Ni_{0.5}Cu_{2.6}B_{5.7}$	0.6	0.102	0.8	0.136	155.1	22.9	283
KA 16	$Ce_{15.1}Fe_{71.8}Co_{5.8}Ni_{0.9}Cu_{2.1}B_{4.3}$	1.2	0.204	0.7	0.119	152.6	24.9	281
KA 17	$Ce_{11.2}Fe_{73.8}Co_{7.8}Ni_{1.3}Cu_{1.7}B_{4.2}$	1.7	0.289	0.7	0.119	140.7	23.8	278
KA 18	$Ce_{14.8}Fe_{68.0}Co_{6.3}Ni_{1.9}Cu_{1.2}B_{7.8}$	2.2	0.374	0.7	0.119	138.1	23.5	282
KA 19	$Ce_{13.7}Fe_{68.8}Co_{6.1}Ni_{2.2}Cu_{0.7}B_{8.5}$	2.4	0.408	0.6	0.102	142.2	24.6	281

either of these two additives. In the case of Ni substitution, the highest M_s and H_a are found to be 135.2 emu/g and 26.6 kOe with T_c of 261 °C, after doping with 0.7 at.% Ni ($x = 0.12$). In contrast, when Cu is doped alone, the M_s and T_c are determined as 133.6 emu/g and 318 °C with H_a of 23.7 kOe after dissolving 0.8 at.% Cu ($y = 0.136$) in $Ce_2Fe_{12.98-y}Co_{1.02}Cu_yB$. A combination of Ni and Cu leads to an enhancement in M_s of $Ce_2Fe_{12.98-x-y}Co_{1.02}Ni_xCu_yB$ ($0.051 \leq x \leq 0.204$, $y \approx 0.119$) which is measured to fall in the range between 147 emu/g and 155 emu/g, with H_a and T_c measured to be close to 24 kOe and 280 °C, respectively.

Acknowledgements

Financial support from General Motors of Canada Ltd., and the Natural Sciences and Engineering Research Council of Canada through the CRD grant program is gratefully acknowledged.

References

[1] J. Fidler, T. Schrefl, S. Hoefinger, M. Hajduga, Recent developments in hard magnetic bulk materials, J. Phys. Condens. Matter 16 (2004) S455–S470.
[2] A.K. Pathak, M. Khan, K.A. Gschneidner Jr., R.W. McCallum, L. Zhou, K. Sun, M.J. Kramer, V.K. Pecharsky, Magnetic properties of bulk, and rapidly solidified nanostructured $(Nd_{1-x}Ce_x)_2Fe_{14-y}Co_yB$ ribbons, Acta Mater. 103 (2016) 211–216.
[3] J.F. Herbst, M.S. Meyer, F.E. Pinkerton, Magnetic hardening of $Ce_2Fe_{14}B$, J. Appl. Phys. 111 (7) (2012) 1–3.
[4] E.J. Skoug, M.S. Meyer, F.E. Pinkerton, M.M. Tessema, D. Haddad, J.F. Herbst, Crystal structure and magnetic properties of $Ce_2Fe_{14-x}Co_xB$ alloys, J. Alloys. Compd. 574 (15) (2013) 552–555.
[5] K. Maaz, A. Mumtaz, S.K. Hasanain, A. Ceylan, Synthesis and magnetic properties of cobalt ferrite ($CoFe_2O_4$) nanoparticles prepared by wet chemical route, J. Magn. Magn. Mater. 308 (2007) 289–295.
[6] T. Wang, D. Kevorkov, M. Medraj, Phase equilibria and magnetic phases in the Ce-Fe-Co-B system, Materials 10 (1) (2017) 16.
[7] Q.M. Lu, M. Yue, H.G. Zhang, M.L. Wang, F. Yu, Q.Z. Huang, D.H. Ryan, Z. Altounian, Intrinsic magnetic properties of single-phase $Mn_{1+x}Ga$ (0<x<1) alloys, Sci. Rep. 5 (2015) 17086–17091.
[8] C.D. Fuerst, E.G. Brewer, Diffusion alloyed additives in die upset Nd-Fe-B magnets, J. Appl. Phys. 69 (8) (1991) 5826–5828.
[9] F. Bolzoni, F. Leccabue, O. Moze, L. Pareti, M. Solzi, Magnetocrystalline anisotropy of Ni and Mn substituted $Nd_2Fe_{14}B$ compounds, J. Magn. Magn. Mater. 67 (3) (1987) 373–377.
[10] A.S. Kim, F.E. Camp, High performance NdFeB magnets (invited), J. Appl. Phys. 79 (8) (1996) 5035–5039.
[11] X'Pert HighScore Plus, PANalytical B.V. Almelo, The Netherlands, 2006, 2.2b (2.2.2). .
[12] H. Putz and K. Brandenburg, Pearson's crystal data, crystal structure database for inorganic compounds, CD-ROM Software Version 1.3.
[13] G. Asti, S. Rinaldi, Nonanaliticity of the magnetization curve: application to the measurement of anisotropy in polycrystalline samples, Phys. Rev. Lett. 28 (24) (1972) 1584–1586.
[14] G. Asti, S. Rinaldi, Singular points in the magnetization curve of a polycrystalline ferromagnet, J. Appl. Phys. 45 (8) (1974) 3600–3610.
[15] X. Liu, D.H. Ryan, M. Wang, Q. Lu, H. Zhang, Experimental and first-principles determination of the magnetocrystalline anisotropy in Mn_xGa, AIP Adv. 7 (2017) 56216–56221.
[16] J.F. Herbst, $R_2Fe_{14}B$ materials: intrinsic properties and technological aspects, Rev. Mod. Phys. 63 (1991) 819–898.
[17] K. Orimoloye, D.H. Ryan, F.E. Pinkerton, M. Medraj, Intrinsic magnetic properties of $Ce_2Fe_{14}B$ modified by Al, Ni, or Si, Appl. Sci. 8 (2) (2018) 205.
[18] F. Sánchez-De Jesús, A.M. Bolarín-Miró, C.A. Cortés Escobedo, G. Torres-Villaseñor, P. Vera-Serna, Structural analysis and magnetic properties of FeCo alloys obtained by mechanical alloying, J. Metall. 2016 (2016) 8347063.
[19] T. Wang, M. Medraj, Magnetic force microscopic study of $Ce_2(Fe, Co)_{14}B$, and its modifications by Ni and Cu, J. Magn. Magn. Mater. 460 (2018) 95–103.
[20] R. Grössinger, X.K. Sun, R. Eibler, K.H.J. Buschow, H.R. Kirchmayr, The temperature dependence of the anisotropy field in $R_2Fe_{14}B$ compounds (R = Y, La, Ce, Pr, Nd, Gd, Ho, Lu), J. Phys. Colloq. 46 (C6) (1985) 221–224.
[21] R. Grössinger, X.K. Sun, R. Eibler, K.H.J. Buschow, H.R. Kirchmayr, Temperature dependence of anisotropy fields and initial susceptibilities in $R_2Fe_{14}B$ compounds, J. Magn. Magn. Mater. 58 (1–2) (1986) 55–60.
[22] M.Q. Huang, E.B. Boltich, W.E. Wallace, Magnetic characteristics of $R_2(Fe, Co)_{14}B$ systems (R=Y, Nd and Gd), J. Magn. Magn. Mater. 60 (1986) 270–274.
[23] N.M. Hong, N.P. Thuy, T.D. Hien, Anomalous anisotropy in the RCo_4B compounds, J. Appl. Phys. 73 (10) (1993) 5917–5919.
[24] J.F. Herbst, W.B. Yelon, Preferential site occupation and magnetic structure of $Nd_2(Co_xFe_{1-x})_{14}B$ systems, J. Appl. Phys. 60 (12) (1986) 4224–4229.
[25] V.L. Dominguez, J.M. Hernàndez, J. Tejada, R.F. Ziolo, Colossal reduction in Curie temperature due to finite-size effects in $CoFe_2O_4$ nanoparticles, Chem. Mater. 25 (1) (2013) 6–11.
[26] L.X. Liao, A. Altounian, D.H. Ryan, Co site preferences in iron rare-earth-based compounds, Phys. Rev. B 47 (17) (1993) 11230–11241.
[27] S.V. Vonsovski, Magnetism, Nauka, Moscow, 1971.
[28] A.A. Lukin, S. Szymura, A.A. Zhuravlyev, S.M. Margaryan, Y.M. Rabinovich, The effect of less additives on magnetic properties and microstructure of sintered Nd-(Fe, Ti, Al)-B magnets, Mater. Chem. Phys. 69 (2001) 284–287.
[29] J.F. Herbst, J.J. Croat, F.E. Pinkerton, W.B. Yelon, Relationships between crystal structure and magnetic properties in $Nd_2Fe_{14}B$, Phys. Rev. B 29 (7) (1984) 4176–4178.
[30] X. Fan, Y. Tang, Z. Shi, M. Jiang, B. Shen, The effect of Ni addition on microstructure and soft magnetic properties of FeCoZrBCu nanocrystalline alloys, AIP Adv. 7 (2017) 056107–056114.
[31] A.R. Denton, N.W. Ashcroft, Vegard's law, Phys. Rev. A 43 (1991) 3161–3164.
[32] S. Dai, A.H. Morrish, X.Z. Zhou, Mössbauer study of the permanent magnet material $Nd_2(Fe_{1-x}Ni_x)_{14}B$, J. Appl. Phys. 63 (1988) 3722–3724.
[33] A.R. Miedema, F.R. de Boer, R. Boom, Model predictions for the enthalpy of formation of transition metal alloys, Calphad 1 (1977) 341–359.
[34] M. Shimizu, J. Inoue, S. Nakagawa, Electronic structure and magnetic properties of Y-Ni intermetallic compounds, J. Phys. F. Met. Phys. 14 (1984) 2673–2687.
[35] Y. Fukuda, A. Fujita, M. Shimotomai, Magnetic properties of monocrystalline $Nd_2(Fe, Co, Ni)_{14}B$, J. Alloys. Compd. 193 (1993) 256–258.
[36] B.D. Cullity, C.D. Graham, Introduction to Magnetic Materials, John Wiley & Sons, 2005.
[37] J.F. Herbst, C.D. Fuerst, R.K. Mishra, C.B. Murphy, D.J. Van Wingerden, Coercivity enhancement of melt-spun Nd-Fe-B ribbons using low-level Cu additions, J. Appl. Phys. 69 (8) (1991) 5823–5825.
[38] H. Okamoto, Phase Diagram of Binary Iron Alloys, ASM International, Materials Park, OH, 1993, pp. 131–137.
[39] M. Palumbo, S. Curiotto, L. Battezzati, Thermodynamic analysis of the stable and metastable Co-Cu and Co-Cu-Fe phase diagrams, Calphad 30 (2006) 171–178.